PNAS RESEARCH ARTICLE | NEUROSCIENCE

Neuronal splicing regulator RBFOX3 mediates seizures via regulating *Vamp1* expression preferentially in NPY-expressing GABAergic neurons

De-Fong Huang[a], Chih-Yu Lee[a,b], Ming-Yi Chou[a], Tzu-Yin Yang[a], Xuhui Cao[a], Yu-Hsuan Hsiao[a], Rui-Ni Wu[a], Cheng-Chang Lien[c], Yi-Shuian Huang[d], Hsiang-Po Huang[b], Susan Shur-Fen Gau[a,e], and Hsien-Sung Huang[a,1]

Edited by Lily Jan, HHMI, University of California, San Francisco, CA; received March 1, 2022; accepted July 2, 2022

Epilepsy is a common neurological disorder, which has been linked to mutations or deletions of RNA binding protein, fox-1 homolog (*Caenorhabditis elegans*) 3 (*RBFOX3*)/*NeuN*, a neuronal splicing regulator. However, the mechanism of seizure mediation by RBFOX3 remains unknown. Here, we show that mice with deletion of *Rbfox3* in gamma-aminobutyric acid (GABA) ergic neurons exhibit spontaneous seizures and high premature mortality due to increased presynaptic release, postsynaptic potential, neuronal excitability, and synaptic transmission in hippocampal dentate gyrus granule cells (DGGCs). Attenuating early excitatory gamma-aminobutyric acid (GABA) action by administering bumetanide, an inhibitor of early GABA depolarization, rescued premature mortality. *Rbfox3* deletion reduced hippocampal expression of vesicle-associated membrane protein 1 (VAMP1), a GABAergic neuron-specific presynaptic protein. Postnatal restoration of VAMP1 rescued premature mortality and neuronal excitability in DGGCs. Furthermore, *Rbfox3* deletion in GABAergic neurons showed fewer neuropeptide Y (NPY)–expressing GABAergic neurons. In addition, deletion of *Rbfox3* in NPY-expressing GABAergic neurons lowered intrinsic excitability and increased seizure susceptibility. Our results establish RBFOX3 as a critical regulator and possible treatment path for epilepsy.

RBFOX3 | Seizure | VAMP1 | NPY | GABAergic neurons

Epilepsy is characterized by recurrent seizures; it has a prevalence of ~8 of 1,000 people, making it one of the most common neurological disorders (1–3). Seizures are primarily generated in the areas of the hippocampus and cerebral cortex. However, details of the pathophysiology of epilepsy remain unclear (4).

RBFOX3 (RNA binding protein, fox-1 homolog [*Caenorhabditis elegans*] 3) is a neuronal alternative splicing regulator (5) that mediates hippocampal circuitry, neurogenesis, and synaptogenesis (6–8). Deletions or mutations of *RBFOX3* were identified in people with epilepsy (9), and a causal relationship has been supported by observations that *Rbfox3* knockout mice exhibit enhanced seizure susceptibility induced by kainic acid (KA) treatment, a well-established model of temporal lobe seizures (7, 10). The hippocampal dentate gyrus (DG) functions as a gatekeeper to prevent hippocampal hyperexcitability and excess synchronization, which can cause temporal lobe seizures (11, 12). It remains unknown how the loss of RBFOX3 in discrete cell types may disrupt the homeostasis of the hippocampal DG and in turn, contribute to epilepsy.

Here, we used conditional *Rbfox3* knockout (KO) mice crossed with 10 different cell type–specific *Cre* mouse lines (gamma-aminobutyric acid (GABA) ergic neurons: *Gad2-Cre*; glutamatergic neurons: *Camk2a-iCre*; hippocampal DG granule cells: *Pomc-Cre*; and seven subtypes of GABAergic neurons: *PV-Cre*, *SOM-Cre*, *VIP-Cre*, *Npy-Cre*, *CR-Cre*, *Cck-Cre*, and *Nos1-Cre*) as models to identify the underlying pathogenic mechanisms of epilepsy that affect people with deletion of *RBFOX3*. We found that selective loss of *Rbfox3* in GABAergic neurons but not glutamatergic neurons was responsible for spontaneous seizures and premature mortality by increasing presynaptic release, postsynaptic potentials, neuronal excitability, and synaptic transmission in granule cells of the hippocampal DG. We rescued seizure phenotypes in *Gad2-Cre/+::Rbfox3*$^{f/f}$ mice by postnatally restoring RBFOX3 or VAMP1 expression in GABAergic neurons or administering bumetanide, an inhibitor of early GABA depolarization. In addition, postnatal restoration of VAMP1 rescued neuronal excitability of hippocampal dentate granule cells. Deletion of *Rbfox3* in GABAergic neurons showed fewer neuropeptide Y (NPY)–expressing GABAergic neurons. Loss of RBFOX3 in NPY-expressing GABAergic neurons has lowered levels of intrinsic excitability compared with controls, which may have contributed to the increased seizure susceptibility exhibited by these mice. Our results provide further insights into the relationship between RBFOX3 and epilepsy as well as the role of RBFOX3 in the pathogenesis of epilepsy.

Significance

Epilepsy is the one of the most common brain disorders globally that affects people of all ages. However, the genetic components of epilepsy are not fully characterized. Here, we identified RNA binding protein, fox-1 homolog (*Caenorhabditis elegans*) 3 (RBFOX3) as a genetic component of epilepsy using mouse genetic approaches in conjunction with genetic and pharmacological rescues. Moreover, RBFOX3 mediates seizure activity in a cell type–specific manner via regulating neuronal viability, intrinsic excitability, excitation/inhibition balance, and the expression of a presynaptic protein. Our work provides mechanistic insights of RBFOX3 into the pathogenesis of epilepsy and the foundation of therapeutics for *RBFOX3*-linked epilepsy.

Author contributions: H.-S.H. designed research; D.-F.H., C.-Y.L., M.-Y.C., T.-Y.Y., X.C., Y.-H.H., R.-N.W., H.-P.H., and S.S.-F.G. performed research; C.-C.L. and Y.-S.H. contributed new reagents/analytic tools; D.-F.H., C.-Y.L., M.-Y.C., T.-Y.Y., X.C., Y.-H.H., and R.-N.W. analyzed data; and H.-S.H. wrote the paper.

The authors declare no competing interest.

This article is a PNAS Direct Submission.

[1]To whom correspondence may be addressed. Email: huang.hsiensung@gmail.com.

This article contains supporting information online at http://www.pnas.org/lookup/suppl/doi:10.1073/pnas.2203632119/-/DCSupplemental.

Published August 11, 2022.

Results

Seizures and Mortality Rates in Mice with Selective Deletion of *Rbfox3* in GABAergic Neurons. Conditional *Rbfox3* knockout mice were generated in which Cre was specifically expressed in GABAergic neurons (*Gad2-Cre*), glutamatergic neurons (*Camk2a-iCre*), and hippocampal granule cells (*Pomc-Cre*) to genetically dissect cell type–specific contributions to circuit imbalance in epilepsy due to the loss of RBFOX3. Deletion of *Rbfox3* in the three cell types was validated with double-immunofluorescence staining of the hippocampal DG using antibodies for GABAergic neurons (anti-GAD1), glutamatergic neurons (anti-CAMK2A), granule cells (anti-PROX1), and RBFOX3 in postnatal day 49 (P49) mice (*Gad2-Cre/+::Rbfox3$^{f/f}$*, *Camk2a-iCre/+::Rbfox3$^{f/f}$*, and *Pomc-Cre/+::Rbfox3$^{f/f}$*) and their littermate controls (*Rbfox3$^{f/f}$* mice) (*SI Appendix*, Fig. S1). The expression patterns of *Gad2-Cre*, *Camk2a-iCre*, and *Pomc-Cre* mice were also validated by profiling fluorescent signals from Cre reporter mice from P0 to P21 (*SI Appendix*, Fig. S2). The onset of Cre expression at P0 was similar for *Gad2-Cre*, *Camk2a-iCre*, and *Pomc-Cre* mice. Thus, our results demonstrate a robust deletion of *Rbfox3* in a cell type–specific manner in the three conditional *Rbfox3* knockout mice.

Although there was no difference in body weight for the three conditional *Rbfox3* knockout mice compared with littermate controls regardless of sex (*SI Appendix*, Fig. S3), mice with selective deletion of *Rbfox3* in GABAergic neurons had a lower rate of survival, with the outcomes being proportional to the degree of *Rbfox3* deletion (*Gad2-Cre/+::Rbfox3$^{f/f}$* < 25%; *Gad2-Cre/+::Rbfox3$^{f/+}$* ∼ 75%), whereas mice with selective deletion of *Rbfox3* in glutamatergic neurons or granule cells or conventional *Rbfox3* knockout mice did not exhibit any change in survival rate (Fig. 1*A*). To confirm that loss of RBFOX3 in GABAergic neurons contributes to a decrease in survival rate, RBFOX3 expression was rescued via an intracerebroventricular (I.C.V.) injection of *adeno-associated virus 9 (AAV9)-Ef1a-DIO-Rbfox3-EYFP* into *Gad2-Cre/+::Rbfox3$^{f/f}$* mice at P0 (Fig. 1 *B*, *Upper*). When compared with control mice injected with *AAV9-Ef1a-DIO-EYFP*, the survival rate was significantly higher for mice following restoration of RBFOX3 (Fig. 1 *B*, *Lower*).

Video recordings were then made of *Gad2-Cre::Rbfox3$^{f/f}$* mice and control counterparts to determine if decreased survival in mice with deletion of *Rbfox3* in GABAergic neurons was due to seizure activity. Spontaneous seizures occurred in 90% of the *Gad2-Cre::Rbfox3$^{f/f}$* mice, and six of nine mice died from the seizures (Fig. 1*C* and Movie S1). KA-induced seizures are widely used as a model of temporal lobe epilepsy (13), and increased seizure susceptibility and severity were observed in conventional *Rbfox3* knockout mice with KA treatment (7). Therefore, to further elucidate the role of selective deletion of *Rbfox3* in GABAergic neurons and seizures, evoked seizure susceptibility with KA was examined. Increased seizure susceptibility with KA was observed following KA treatment in *Gad2-Cre/+::Rbfox3$^{f/f}$* mice with selective deletion of *Rbfox3* in GABAergic neurons (Fig. 1*D*) but not in *Camk2a-iCre/+::Rbfox3$^{f/f}$* mice with deletion of *Rbfox3* in glutamatergic neurons (Fig. 1*E*). Collectively, our data indicate that RBFOX3 in GABAergic neurons mediates seizure susceptibility.

Increased Neuronal Excitability and Synaptic Transmission in Hippocampal Granule Cells following Selective Deletion of *Rbfox3* in GABAergic Neurons. To address neuronal mechanisms of spontaneous seizures caused by *Rbfox3* deletion in GABAergic neurons of mice, we targeted the hippocampal DG, which serves as a filter for protecting neurons against hyperexcitability and excess synchronization leading to temporal lobe seizures (11). Paired-pulse ratio (PPR) measured in the dentate gyrus granule cells (DGGCs) in hippocampal slices with the stimulating electrode positioned in the medial perforant path from the three different P49 conditional *Rbfox3* knockout (*Gad2-Cre/+::Rbfox3$^{f/f}$*, *Camk2a-iCre/+::Rbfox3$^{f/f}$*, and *Pomc-Cre/+::Rbfox3$^{f/f}$*) and control (*Rbfox3$^{f/f}$*) mice under physiological conditions (Fig. 1 *F*, *Left*) demonstrated a decreased PPR in neurons from *Gad2-Cre/+::Rbfox3$^{f/f}$* mice (Fig. 1 *F*, *Center*). When observed evoked postsynaptic potential (ePSP) in hippocampal DGGCs with the stimulating electrode positioned in the medial perforant path from the three P49 conditional *Rbfox3* knockout and control mice under physiological conditions was determined, the amplitude of the ePSP from *Gad2-Cre/+::Rbfox3$^{f/f}$* mice was higher than that from *Rbfox3* controls and the other two conditional *Rbfox3* knockouts (Fig. 1 *F*, *Right*). To further address the increased amplitude of the ePSP from *Gad2-Cre/+::Rbfox3$^{f/f}$* mice, we recorded light-evoked inhibitory postsynaptic currents (eIPSCs) in DGGCs with optogenetic stimulation in surrounding GABAergic neurons from *Gad2-Cre/+::Rbfox3$^{f/f}$::mDlx-ChR2* mice. We observed a decreased area but no change in amplitude of eIPSCs in DGGCs from *Gad2-Cre/+::Rbfox3$^{f/f}$::mDlx-ChR2* mice compared with their corresponding controls (*SI Appendix*, Fig. S4). Next, neuronal excitability of DGGCs was measured on P49 hippocampal slices from the three different conditional *Rbfox3* knockout and control mice under physiological conditions (without any synaptic transmission blockers) (Fig. 1 *G*, *Left*). Increased neuronal excitability of DGGCs was observed in hippocampal slices from *Gad2-Cre/+::Rbfox3$^{f/f}$* mice (Fig. 1 *G*, *Center* and *Right*) as well as increased hyperpolarization and shortened action potential duration (*SI Appendix*, Fig. S5). To further investigate whether increased neuronal excitability can be observed in young *Gad2-Cre/+::Rbfox3$^{f/f}$* mice, we examined neuronal excitability of DGGCs in hippocampal slices from *Gad2-Cre/+::Rbfox3$^{f/f}$* mice at P21. We indeed observed increased neuronal excitability in young *Gad2-Cre/+::Rbfox3$^{f/f}$* mice (*SI Appendix*, Fig. S6). Our results indicate that hippocampal DGGCs from *Gad2-Cre/+::Rbfox3$^{f/f}$* mice are more excitable compared with DGGCs from *Camk2a-iCre/+::Rbfox3$^{f/f}$* and *Pomc-Cre/+::Rbfox3$^{f/f}$* conditional knockout mice or *Rbfox3$^{f/f}$* controls. In addition, abnormal patterns of action potentials occurred in DGGCs from *Gad2-Cre/+::Rbfox3$^{f/f}$* mice.

RBFOX3 Mediates Excitation/Inhibition Balance in a Cell Type–Specific Manner. Excitatory and/or inhibitory inputs could be important for the increased neuronal excitability of the hippocampal DGGCs observed in *Gad2-Cre/+::Rbfox3$^{f/f}$* mice (Fig. 1*G*). Therefore, firing rates of DGGCs in *Gad2-Cre/+::Rbfox3$^{f/f}$* and control (*Rbfox3$^{f/f}$*) mice were measured after blocking these inputs. We observed normal firing rates with abnormal intrinsic properties in hippocampal DGGCs from *Gad2-Cre/+::Rbfox3$^{f/f}$* mice compared with controls (*SI Appendix*, Fig. S7). These results indicate an imbalance in excitation/inhibition that could be explained, in part, by changes in neuronal excitability of hippocampal DGGCs in *Gad2-Cre/+::Rbfox3$^{f/f}$* mice.

To further investigate how RBFOX3 regulates excitation and inhibition inputs in a cell type–specific manner, we measured the frequency and amplitude of miniature inhibitory postsynaptic currents (mIPSCs) with patch-clamp recordings in hippocampal DGGCs from the three conditional *Rbfox3* knockout and control mice at P49 (Fig. 2*A*). There was an increase in frequency but not amplitude for mIPSCs in hippocampal DGGCs from *Gad2-Cre/+::Rbfox3$^{f/f}$* mice (Fig. 2*A*). Moreover, a slight

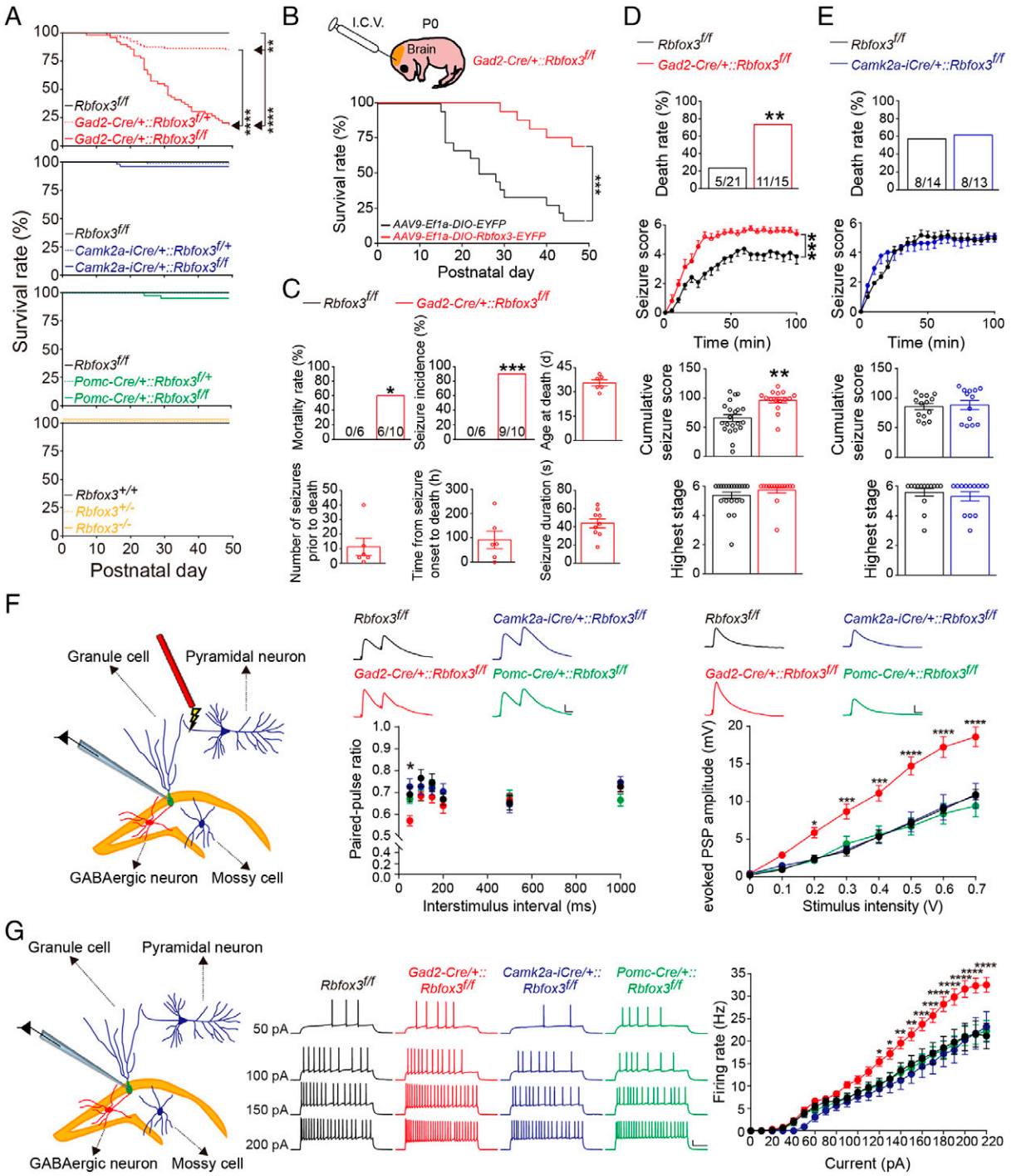

Fig. 1. Selective deletion of *Rbfox3* in GABAergic but not glutamatergic neurons causes spontaneous seizures and higher mortality in mice and increased neuronal excitability and synaptic transmission in hippocampal granule cells. (*A*) Survival rate of mice from P0 to P49: *Gad2-Cre/+::Rbfox3$^{f/f}$* (n = 49), *Gad2-Cre/+::Rbfox3$^{f/+}$* (n = 81), *Rbfox3$^{f/f}$* (n = 45), *Camk2a-iCre/+::Rbfox3$^{f/f}$* (n = 55), *Camk2a-iCre/+::Rbfox3$^{f/+}$* (n = 90), *Rbfox3$^{f/f}$* (n = 31), *Pomc-Cre/+::Rbfox3$^{f/f}$* (n = 39), *Pomc-Cre/+::Rbfox3$^{f/+}$* (n = 43), *Rbfox3$^{f/f}$* (n = 43), *Rbfox3$^{-/-}$* (n = 33), *Rbfox3$^{+/-}$* (n = 25), and *Rbfox3$^{+/+}$* (n = 23). Log-rank test with the Holm–Sidak post hoc comparison. (*B*, *Upper*) Schematic of the I.C.V. injection at P0 of *AAV9-DIO-Rbfox3-EYFP* or *AAV9-DIO-EYFP* in *Gad2-Cre/+::Rbfox3$^{f/f}$* mice (n = 16 for *AAV9-DIO-Rbfox3-EYFP*; n = 18 for *AAV9-DIO-EYFP*). (*B*, *Lower*) Graph demonstrating the survival rate of mice from P0 to P49. Log-rank test with the Holm–Sidak post hoc test. (*C*) Parameters of spontaneous seizures for *Gad2-Cre/+::Rbfox3$^{f/f}$* mice (n = 10) and controls (*Rbfox3$^{f/f}$*; n = 6) were analyzed from video recordings. Student's t test (two tailed). Parameters of seizure susceptibility were measured 100 min after KA treatment: (*D*) *Gad2-Cre/+::Rbfox3$^{f/f}$* mice (n = 15) and controls (*Rbfox3$^{f/f}$*; n = 21) and (*E*) *Camk2a-iCre/+::Rbfox3$^{f/f}$* mice (n = 13) and controls (*Rbfox3$^{f/f}$*; n = 14). Student's t test (two tailed) or two-way repeated measures ANOVA with the Holm–Sidak post hoc comparison. (*F*) Paired-pulse depression and ePSP. Schematic of experiments in which the stimulating electrode was positioned in the medial perforant path and the recording electrode was positioned in the hippocampal DGGCs (*Left*); representative traces from 50-ms interpulse intervals (*Upper Center*) and analysis of PPR at varying intervals (*Lower Center*). *Rbfox3$^{f/f}$* mice, n = 18 cells from five mice; *Gad2-Cre/+::Rbfox3$^{f/f}$* mice, n = 24 cells from six mice; *Camk2a-iCre/+::Rbfox3$^{f/f}$* mice, n = 20 cells from six mice; *Pomc-Cre/+::Rbfox3$^{f/f}$* mice, n = 26 cells from seven mice. Representative traces of ePSP at 0.7-V stimulus intensity (*Upper Right*) and analysis at varying intensities (*Lower Right*). *Rbfox3$^{f/f}$* mice, n = 15 cells from five mice; *Gad2-Cre/+::Rbfox3$^{f/f}$* mice, n = 21 cells from six mice; *Camk2a-iCre/+::Rbfox3$^{f/f}$* mice, n = 17 cells from five mice; *Pomc-Cre/+::Rbfox3$^{f/f}$* mice, n = 22 cells from five mice. Two-way repeated measures ANOVA with the Holm–Sidak post hoc comparison. (Scale bars: 2 mV and 10 ms.) (*G*) Representative responses to current injections and average spike frequency–current curves in DGGCs: *Rbfox3$^{f/f}$* mice, n = 14 cells from five mice; *Gad2-Cre/+::Rbfox3$^{f/f}$* mice, n = 21 cells from six mice; *Camk2a-iCre/+::Rbfox3$^{f/f}$* mice, n = 12 cells from five mice; *Pomc-Cre/+::Rbfox3$^{f/f}$* mice, n = 18 cells from six mice. Two-way repeated measures ANOVA with the Holm–Sidak post hoc comparison (Scale bars: 20 mV and 200 ms). Data are presented as mean ± SEM. *P < 0.05; **P < 0.01; ***P < 0.001; ****P < 0.0001.

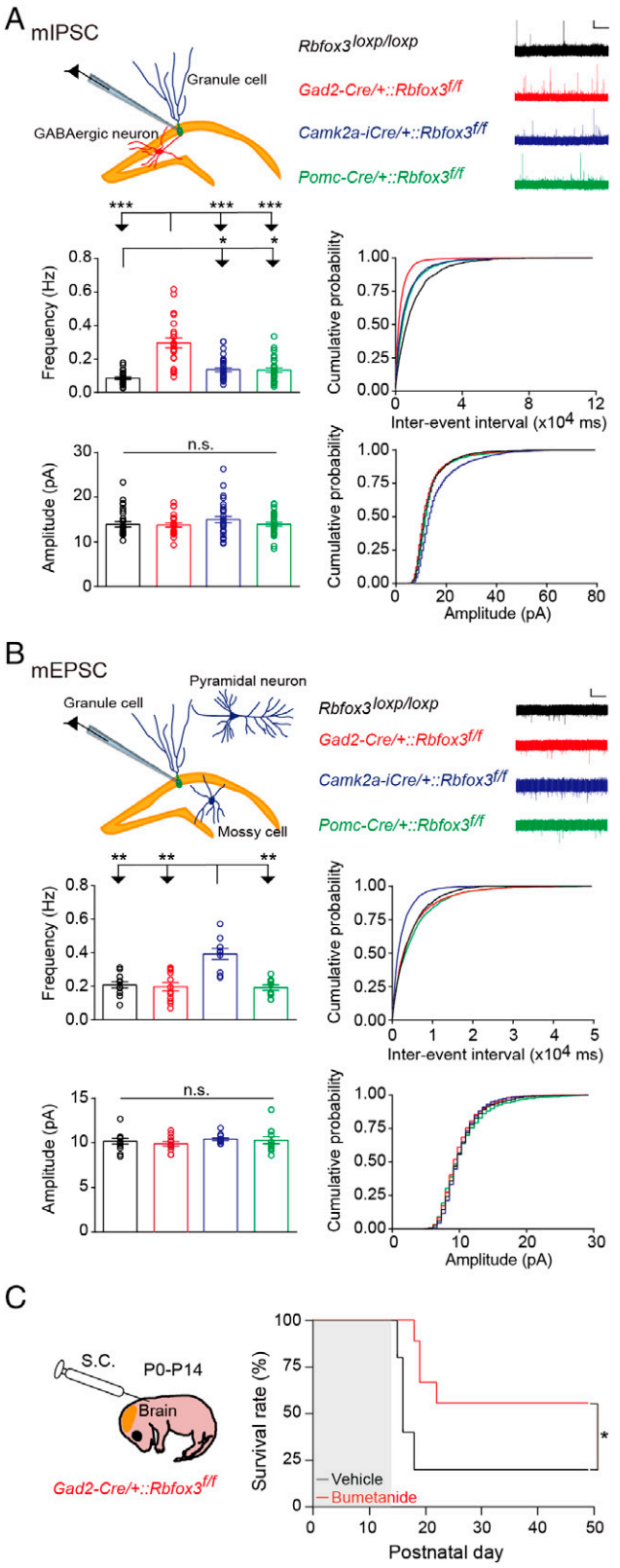

Fig. 2. Increased frequency of inhibitory neurotransmission but normal frequency of excitatory neurotransmission in granule cells of adult *Gad2-Cre::Rbfox3$^{f/f}$* mice with seizure susceptibility rescued by bumetanide. (*A*) Schematic of patch-clamp recordings of granule cells in hippocampal slices for mIPSC (*Top Left*). Representative traces from recordings of mIPSC (*Top Right*). Frequency and interevent interval cumulative probability are shown for mIPSC (*Middle Left* and *Middle Right*, respectively). Amplitude and cumulative probability are shown for mIPSC (*Bottom Left* and *Bottom Right*, respectively). mIPSC: *Rbfox3$^{f/f}$*, n = 30 cells from five mice; *Gad2-Cre/+::Rbfox3$^{f/f}$*, n = 23 cells from four mice; *Camk2a-iCre/+::Rbfox3$^{f/f}$*, n = 32 cells from five mice; *Pomc-Cre/+::Rbfox3$^{f/f}$*, n = 32 cells from five mice. Kruskal–Wallis one-way ANOVA on ranks with Dunn's post hoc test. (Scale bar: 10 pA and 10 s). (*B*) Schematic of patch-clamp recordings of granule cells in hippocampal slices for mEPSC (*Top Left*). Representative traces from recordings of mEPSC (*Top Right*). Frequency and interevent interval cumulative probability are shown for mEPSC (*Middle Left* and *Middle Right*, respectively). Amplitude and cumulative probability are shown for mEPSC (*Bottom Left* and *Bottom Right*, respectively). mEPSC: *Rbfox3$^{f/f}$*, n = 12 cells from five mice; *Gad2-Cre/+::Rbfox3$^{f/f}$*, n = 12 cells from four mice; *Camk2a-iCre/+::Rbfox3$^{f/f}$*, n = 12 cells from five mice; *Pomc-Cre/+::Rbfox3$^{f/f}$*, n = 12 cells from five mice. Kruskal–Wallis one-way ANOVA on ranks with Dunn's post hoc test. (Scale bar: 10 pA and 10 s). (*C, Left*) Schematic of S.C. injection of bumetanide or vehicle administered twice per day from P0 to P14 in *Gad2-Cre/+::Rbfox3$^{f/f}$* mice (n = 16 for bumetanide; n = 14 for vehicle). (*C, Right*) Survival rate of mice following injection of bumetanide (red) or vehicle (black) from P0 to P49. Log-rank test with the Holm–Sidak post hoc test. All data are presented as mean ± SEM. n.s., nonsignificant. *P < 0.05; **P < 0.01; ***P < 0.001.

but significant increase was observed in frequency, but not amplitude, of mIPSCs in hippocampal DGGCs from *Camk2a-iCre/+::Rbfox3$^{f/f}$* and *Pomc-Cre/+::Rbfox3$^{f/f}$* mice (Fig. 2*A*). When the frequency and amplitude were measured for miniature excitatory postsynaptic currents (mEPSCs) from the three conditional knockout and control mice at P49 (Fig. 2*B*), the observed frequency of mEPSCs in hippocampal DGGCs from *Camk2a-iCre::Rbfox3$^{f/f}$* mice was greater than for the other mice; however, there was no increase in amplitude (Fig. 2*B*).

Based on the increased frequency of mIPSCs, but not mEPSC, in hippocampal DGGCs from *Gad2-Cre/+::Rbfox3$^{f/f}$* mice (Fig. 2*A*), we hypothesized that excess excitatory GABA actions from GABAergic neurons with deletion of *Rbfox3* in the very early stages of neurodevelopment contribute to seizures. Therefore, we administered bumetanide, an inhibitor of GABA-mediated depolarization, which prevents hyperexcitability and seizure-like behaviors (14). Injections of bumetanide subcutaneously (S.C.) into mice with selective deletion of *Rbfox3* in GABAergic neurons twice per day for 14 d (P0 to P14) (Fig. 2 *C, Left*) successfully rescued seizure phenotypes and increased survival rates (Fig. 2 *C, Right*). This result was equivalent to selectively restoring RBFOX3 expression in GABAergic neurons (Fig. 1*B*). Taken together, these results demonstrate that RBFOX3 regulates the balance of neuronal and synaptic excitation and inhibition in a cell type–specific manner.

Premature Mortality and Neuronal Excitability Are Rescued by Postnatal Restoration of VAMP1 in Mice with *Rbfox3* Deletion in GABAergic Neurons. Known and related seizure susceptibility genes could be downstream targets of RBFOX3. Therefore, a panel of seizure-related candidate genes was searched using qPCR analysis of the hippocampus from *Rbfox3* conventional homozygous knockout (Homo) and control wild-type (WT) mice (Datasets S1 and S2). Levels of messenger ribonucleic acid (mRNA) for *Vamp1* were significantly lower in the hippocampus of Homo mice compared with their WT controls (Fig. 3*A*). Five 3′ untranslated region (UTR) sites for *Vamp1* mRNA were specifically bound by RBFOX3 (Fig. 3 *A, Upper* and Dataset S3) (15), and protein levels of VAMP1 were significantly lower in hippocampal extracts from Homo mice compared with their WT controls (Fig. 3*B*). VAMP1 is a GABAergic neuron-specific presynaptic vesicle-associated protein. Loss of VAMP1 has been shown to be associated with seizure phenotypes (16). To confirm whether decreased VAMP1 in GABAergic neurons is required for spontaneous seizures, we specifically restored VAMP1 expression in GABAergic neurons with deletion of *Rbfox3* via an I.C.V. injection of *AAV9-Ef1a-DIO-Vamp1-EYFP* into *Gad2-Cre/+::Rbfox3$^{f/f}$* mice at P0 (Fig. 3 *C, Upper*). When compared with control mice injected with *AAV9-Ef1a-DIO-EYFP*, survival rates

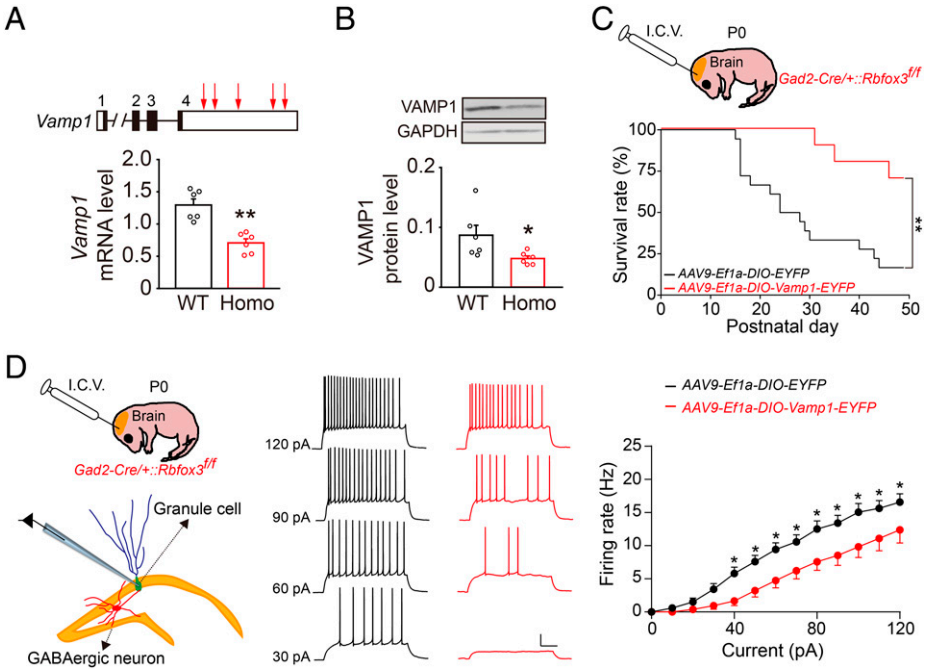

Fig. 3. RBFOX3 regulates *Vamp1* expression, and restoration of VAMP1 rescues seizure susceptibility in mice with deletion of *Rbfox3* in GABAergic neurons. (*A* and *B*) RNA and protein analyses from the hippocampus of *Rbfox3* Homo mice and their WT counterparts. (*A*) qPCR analysis of *Vamp1*. Red arrows indicate in vivo RBFOX3 binding sites. (*B*) Western blot analysis of VAMP1. The Mann–Whitney rank sum test or Student's *t* test (two tailed). $n = 5$ to 7 per group. (*C, Upper*) Schematic of I.C.V. injection at P0 of *AAV9-DIO-Vamp1-EYFP* or *AAV9-DIO-EYFP* in *Gad2-Cre/+::Rbfox3$^{f/f}$* mice ($n = 10$ for *AAV9-DIO-Vamp1-EYFP*; $n = 18$ for *AAV9-DIO-EYFP*) at P0. (*C, Lower*) Survival rate following injection of *AAV9-DIO-Vamp1-EYFP* (red) or *AAV9-DIO-EYFP* (black) in *Gad2-Cre/+::Rbfox3$^{f/f}$* mice from P0 to P49. Log-rank test with the Holm–Sidak post hoc test. (*D*) Schematic of I.C.V. injection at P0 of *AAV9-DIO-Vamp1-EYFP* or *AAV9-DIO-EYFP* in *Gad2-Cre/+::Rbfox3$^{f/f}$* mice. Representative responses to current injections and average spike frequency–current curves of DGGCs following injection of *AAV9-DIO-Vamp1-EYFP* (red; $n = 23$ cells from four mice) or *AAV9-DIO-EYFP* (black; $n = 35$ cells from seven mice) in *Gad2-Cre/+::Rbfox3$^{f/f}$* mice at P21. Two-way repeated measures ANOVA with the Holm–Sidak post hoc comparison. All data are presented as mean ± SEM. (Scale bar: 20 mV and 200 ms.) $^*P < 0.05$; $^{**}P < 0.01$.

were significantly higher following injection of *AAV9-Ef1a-DIO-Vamp1-EYFP*, providing further evidence that VAMP1 is associated with seizure phenotypes (Fig. 3 *C*, *Lower*). Moreover, postnatal restoration of VAMP1 also rescued neuronal excitability of hippocampal dentate granule cells with *Rbfox3* deletion in GABAergic neurons (Fig. 3*D*). Our results showed that decreased expression of VAMP1 contributes to increased neuronal excitability and in turn, seizure behaviors in mice with *Rbfox3* deletion in GABAergic neurons.

Alterations in the Number of Hippocampal GABAergic Neurons with Deletion of *Rbfox3*. The hippocampal DG is composed of a heterogenous population of GABAergic and glutamatergic neurons (17–21). Analysis of neuronal subtypes with the Allen Brain Atlas Transcriptomics Explorer demonstrated that *Rbfox3* was disproportionally expressed in GABAergic neurons (Fig. 4 *A* and *B*). Loss of hippocampal GABAergic interneurons has been described in human temporal lobe epilepsy and mouse models of epilepsy (22). To address whether loss of GABAergic neurons plays a role in the development of spontaneous seizures in mice, we used immunofluorescent quantification of neurons in the hippocampal DG sections of Cre reporter mice (*Gad2-Cre/+::Rbfox3$^{f/f}$::Ai14* mice) and controls (*Gad2-Cre/+::Rbfox3$^{+/+}$::Ai14* mice), in which all GABAergic neurons express tdTomato red signal labeled with subtype-specific antibodies (neuropeptide Y [NPY], calretinin [CR], cholecystokinin [CCK], parvalbumin [PV], somatostatin [SOM], vasoactive intestinal polypeptide [VIP], and nitric oxide synthase 1 [NOS1]). Bar graphs in Fig. 4*C* shows fewer NPY-, SOM-, and NOS1-expressing GABAergic neurons in the hippocampal DG from *Gad2-Cre/+::Rbfox3$^{f/f}$::Ai14* mice compared with controls; in contrast, there were more CR-expressing GABAergic neurons in the outer molecular layer and fewer in the hilus of the hippocampal DG from *Gad2-Cre/+::Rbfox3$^{f/f}$::Ai14* mice compared with controls. There was no significant difference in the number of CCK-, PV-, and VIP-expressing neurons between *Gad2-Cre/+::Rbfox3$^{f/f}$::Ai14* mice and controls. Thus, the absence of *Rbfox3* resulted in variations of the cell number in the four subtypes of GABAergic neurons when compared with controls: NPY, SOM, NOS1, and CR.

Reduced expression levels of markers for the seven GABAergic neurons subtypes may contribute to a decrease of their immunoactivities. Therefore, to rule out this possibility, changes in expression levels for markers of the seven GABAergic neuron subtypes were compared for *Rbfox3* Homo with WT mice. RNA expression levels for markers of subtypes did not differ between Homo and WT mice (Dataset S1). Our results suggest that deletion of *Rbfox3* in GABAergic neurons alters the number of cells in a subtype-specific manner, which could also contribute to seizure susceptibility in a subtype-specific manner.

The Most Severe Seizures Were Exhibited by Mice with Selective Deletion of *Rbfox3* in NPY-Expressing GABAergic Neurons. To further identify which GABAergic neuron subtype with *Rbfox3* deletion contributes significantly to the development of seizures, we examined KA-induced seizures in conditional *Rbfox3* knockout mouse lines with selective *Rbfox3* deletion in seven subtypes of GABAergic neurons. The most significantly increased seizure susceptibility following treatment with KA was observed in *Npy-Cre/+::Rbfox3$^{f/f}$* mice compared with controls (Fig. 5*B*). We also observed an increase in seizure phenotypes compared with controls in *CR-Cre/+::Rbfox3$^{f/f}$* mice (Fig. 5*C*) and *PV-Cre/PV-Cre::SOM-Cre/+::Rbfox3$^{f/f}$* mice (Fig. 5*D*). Seizure phenotypes were lower compared with controls for *Cck-Cre/+::Rbfox3$^{f/f}$* mice (Fig. 5*E*). There was

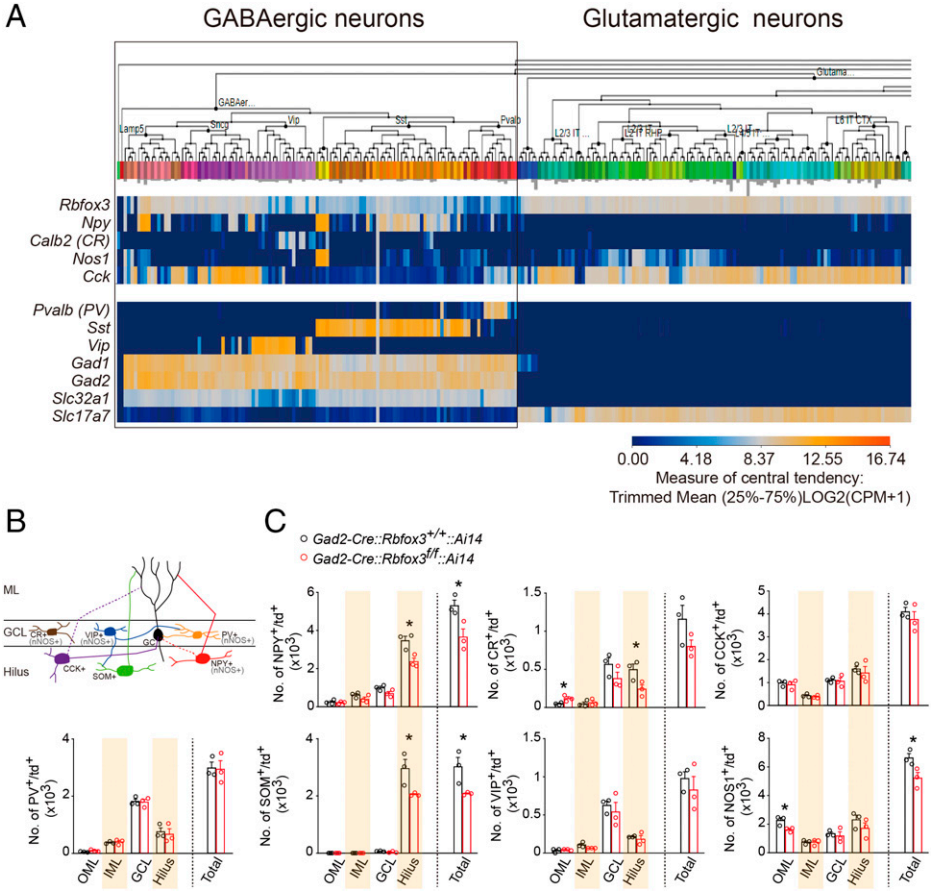

Fig. 4. Deletion of *Rbfox3* in GABAergic neurons results in altered numbers of neuronal subtypes in mice. (*A*) Expression levels of *Rbfox3* in GABAergic neurons and glutamatergic neurons were compared using the Transcriptomics Explorer from the Allen Brain Atlas. (*B*) Schematic diagram of the seven subtypes of GABAergic neurons expressing *Rbfox3* in the hippocampal DG. (*C*) Bar graphs indicate the number of positive cells counted in the different layers of hippocampal DG from GABAergic neurons from *Gad2-Cre/+::Rbfox3*$^{f/f}$*::Ai14* mice (red) and controls (*Gad2-Cre/+::Rbfox3*$^{+/+}$*::Ai14* mice; black) for the seven subtypes. Mann–Whitney rank sum test or Student's *t* test (two tailed). $n = 6$ to 8 sections/mouse, three mice per group. All data are presented as mean ± SEM. GCL, granule cell layer; IML, inner molecular layer; OML, outer molecular layer; ML, molecular layer; CPM, count per million. *$P < 0.05$.

no difference in seizure susceptibility compared with controls for *PV-Cre/+::Rbfox3*$^{f/f}$ mice (Fig. 5*F*), *SOM-Cre/+::Rbfox3*$^{f/f}$ mice (Fig. 5*G*), *PV-Cre/+::SOM-Cre/+::Rbfox3*$^{f/f}$ mice (*SI Appendix*, Fig. S8*A*), or *PV-Cre/PV-Cre::Rbfox3*$^{f/f}$ mice (*SI Appendix*, Fig. S8*B*). We included *PV-Cre/PV-Cre::Rbfox3*$^{f/f}$ mice because *Cre* has been reported to not be fully expressed in heterozygous *PV-Cre* mice (23). No spontaneous seizures were detected over 2 wk by video monitoring mice from P22 in *PV-Cre/+::Rbfox3*$^{f/f}$ mice ($n = 9$ for WT; $n = 9$ for KO) and *SOM-Cre/+::Rbfox3*$^{f/f}$ mice ($n = 9$ for WT; $n = 9$ for KO) with their corresponding controls. There was no difference compared with controls in seizure susceptibility in *VIP-Cre/+::Rbfox3*$^{f/f}$ (Fig. 5*H*) and *Nos1-Cre/+::Rbfox3*$^{f/\Delta}$ mice (Fig. 5*I*) or the survival rates of mice with selective *Rbfox3* deletion in seven subtypes of GABAergic neurons (*SI Appendix*, Fig. S9). Our data demonstrate that selective deletion of *Rbfox3* in NPY-expressing GABAergic neurons contributes more significantly to increased seizure susceptibility compared with other subtypes of GABAergic neurons.

Selective Loss of *Rbfox3* in NPY-Expressing GABAergic Neurons Decreases Intrinsic Excitability. Our findings indicated that selective deletion of *Rbfox3* in NPY-expressing GABAergic neurons contributed to the most significant seizure phenotypes (Fig. 5*B*), which suggested that neuronal intrinsic excitability in NPY-expressing GABAergic neurons might be affected by the loss of RBFOX3. Indeed, when NPY-expressing GABAergic neurons with *Rbfox3* deletion were compared with controls, neuronal intrinsic excitability in the hippocampus was significantly lower for *Npy-Cre/+::Rbfox3*$^{f/f}$*::Ai14* mice compared with their corresponding controls (Fig. 6*A*). We also examined neuronal intrinsic excitability in three major subtypes of GABAergic neurons using *PV-*, *SOM-*, and *VIP-Cre* mice with selective deletion of *Rbfox3*. We observed a higher level of intrinsic excitability in PV-expressing GABAergic neurons; no differences were observed in SOM- and VIP-expressing GABAergic neurons with *Rbfox3* deletion (Fig. 6 *C–E*, respectively). To test whether excitability of GABAergic neurons with cell type–specific deletion of *Rbfox3* can be reproduced in *Gad-Cre/+::Rbfox3*$^{f/+}$ mice, we recorded NPY-expressing GABAergic neurons, PV-expressing GABAergic neurons, and non-PV-expressing GABAergic neurons in the hippocampus of *Gad2-cre/+::Rbfox3*$^{f/+}$*::Ai14/+* mice based on the location, morphology, and electrophysiological properties of GABAergic neurons (24, 25). We observed the same patterns of neuronal excitability of the above three types of GABAergic neurons as the findings in Fig. 6 (*SI Appendix*, Fig. S10). Overall, these results suggest that decreased neuronal intrinsic excitability occurs in NPY-expressing GABAergic neurons with deletion of *Rbfox3*, which could decrease NPY-expressing GABAergic neuron-mediated inhibition and then, contribute to increased seizure susceptibility.

Discussion

Mutations or deletions in *RBFOX3* have been linked to epilepsy. Our study provides evidence for cell type–specific contributions

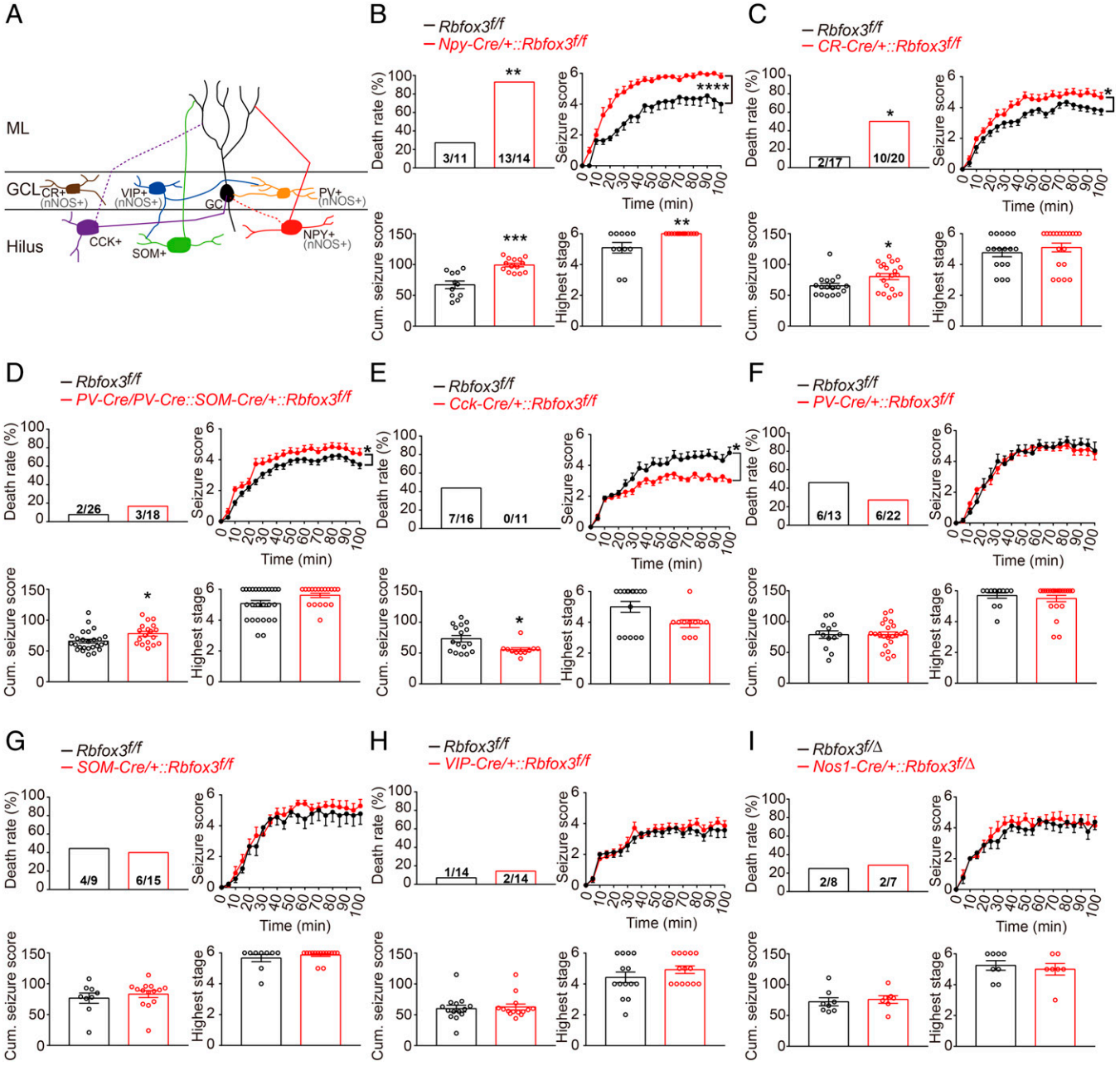

Fig. 5. Selective *Rbfox3* deletion in NPY-expressing GABAergic neurons displays increased seizure susceptibility. (*A*) Schematic diagram of the seven subtypes of GABAergic neurons in the hippocampal DG. GCL, granule cell layer. (*B–I*) Seizure susceptibility observed over 100 min following treatment with KA. KA was administered to *Npy-Cre/+ (B), CR-Cre/+ (C), Cck-Cre/+ (D), PV-Cre/PV-Cre::SOM-Cre/+ (E), PV-Cre/+ (F), SOM-Cre/+ (G), VIP-Cre/+ (H), and Nos1-Cre/+ (I)::Rbfox3f/f* mice (red) respectively and their corresponding controls (black). Sample size is indicated at the bottom of each bar. Two-way repeated measures ANOVA with the Holm–Sidak post hoc comparison or Student's *t* test (two tailed). All data are presented as mean ± SEM. **P* < 0.05; ***P* < 0.01; ****P* < 0.001; *****P* < 0.0001. ML: molecular layer.

to the neurobiology of epilepsy for RBFOX3 at the level of subtypes of GABAergic neurons. Our results showed that mice with *Rbfox3* deletion in GABAergic neurons developed spontaneous seizures with a high mortality rate, which was driven by a dysregulation in the balance between excitation and inhibition. Seizures in mice with *Rbfox3* deletion in GABAergic neurons were rescued in postnatal mice by restoring RBFOX3 or VAMP1 expression in GABAergic neurons or administering bumetanide. Restoration of VAMP1 rescued the neuronal excitability of hippocampal dentate granule cells from mice with *Rbfox3* deletion in GABAergic neurons. Mice with deletion of *Rbfox3* in GABAergic neurons showed a fewer number of NPY-expressing GABAergic neurons than their controls. Therefore, a reduction in NPY-expressing GABAergic neuron-mediated inhibition could contribute to higher seizure susceptibility.

Neuronal excitability of granule cells in *Gad2-Cre/+::Rbfox3$^{f/f}$* mice under physiological conditions was significantly higher than granule cells from control mice, which returned to normal levels by blocking of excitatory and inhibitory synaptic inputs. These results strongly suggested that GABAergic RBFOX3 does not affect the intrinsic excitability of granule cells per se but mediates the balance of synaptic transmission from excitatory and inhibitory inputs. Further support for GABAergic RBFOX3 as a mediator for synaptic transmission stems from our findings demonstrating an increased inhibitory synaptic transmission in *Gad2-Cre/+::Rbfox3$^{f/f}$* mice. In addition, although there was no

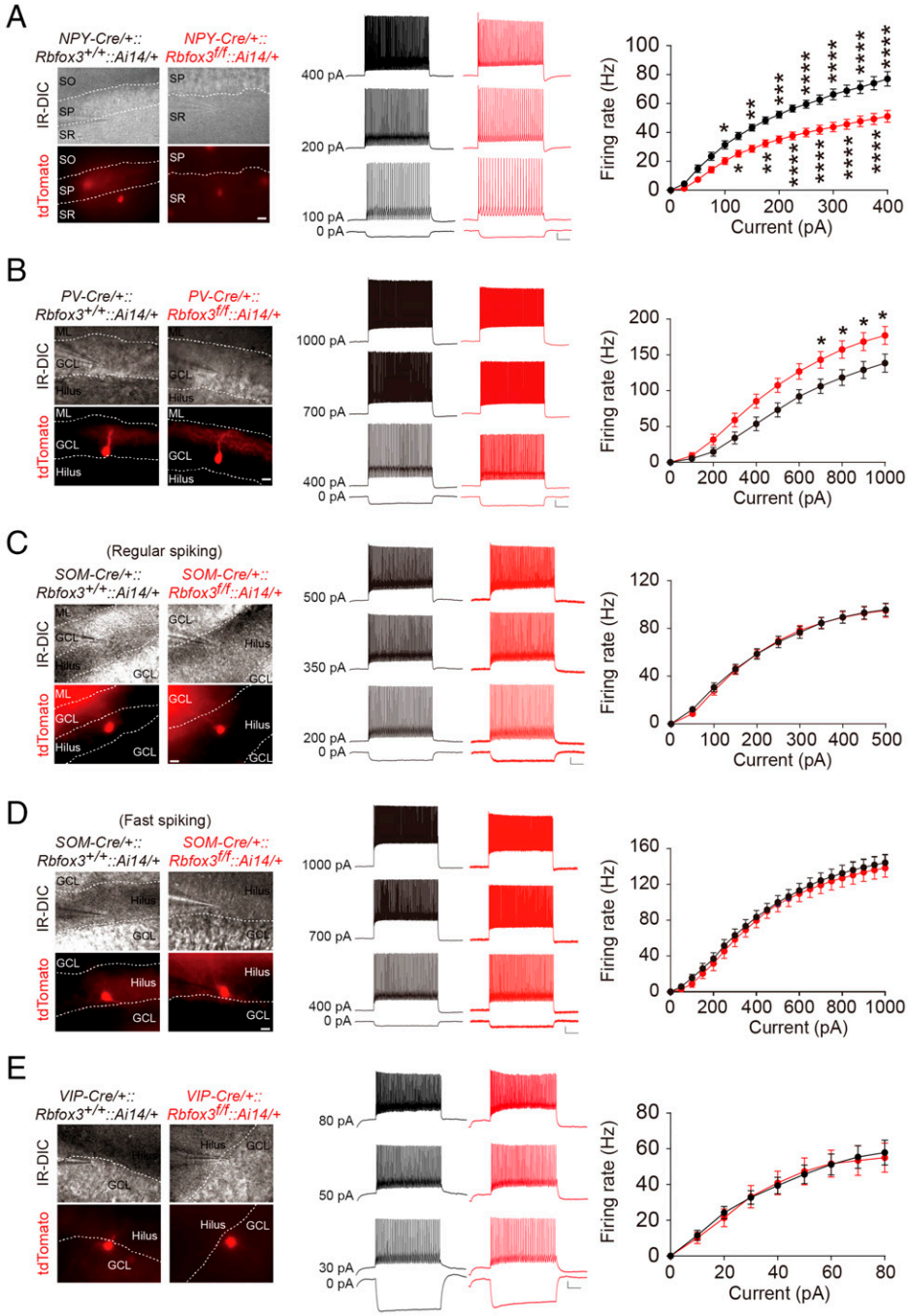

Fig. 6. Selective *Rbfox3* deletion in NPY-expressing GABAergic neurons displaying decreased intrinsic excitability in the mouse hippocampus. (*A*, *Left*, *B*, *Left*, *C*, *Left*, *D*, *Left*, and *E*, *Left*) Representative images of cells in the hippocampus for control (black) and *Rbfox3* deletion in specific subtypes of GABAergic neurons (red) photographed in infrared (IR-DIC; *A*, *Upper Left*, *B*, *Upper Left*, *C*, *Upper Left*, *D*, *Upper Left*, and *E*, *Upper Left*) and fluorescence (*A*, *Lower Left*, *B*, *Lower Left*, *C*, *Lower Left*, *D*, *Lower Left*, and *E*, *Lower Left*). (*A*, *Center*, *B*, *Center*, *C*, *Center*, *D*, *Center*, and *E*, *Center*) Representative traces of neuronal response to current injection of GABAergic neurons. (*A*, *Right*, *B*, *Right*, *C*, *Right*, *D*, *Right*, and *E*, *Right*) Graphs showing average spike frequency–current curves. (*A*) NPY-expressing cells (control, $n = 14$ cells from four mice; *NPY-Cre/+::Rbfox3$^{f/f}$::Ai14*, $n = 14$ cells from three mice). (*B*) PV-expressing cells (control, $n = 15$ cells from 10 mice; *PV-Cre/+::Rbfox3$^{f/f}$::Ai14*, $n = 16$ cells from 8 mice). (*C*) SOM-expressing cells with regular spiking (control, $n = 26$ cells from 18 mice; *SOM-Cre/+::Rbfox3$^{f/f}$::Ai14*, $n = 25$ cells from 15 mice). (*D*) SOM-expressing cells with fast spiking (control, $n = 18$ cells from 13 mice; *SOM-Cre/+::Rbfox3$^{f/f}$::Ai14*, $n = 14$ cells from 9 mice). (*E*) VIP-expressing interneurons (control, $n = 9$ cells from four mice; *VIP-Cre/+::Rbfox3$^{f/f}$::Ai14*, $n = 9$ cells from six mice). Two-way repeated measures ANOVA with the Holm–Sidak post hoc comparison. All data are presented as mean ± SEM. GCL, granule cell layer. (Scale bars: 20 μm for representative fluorescent images; 20 mV and 200 ms for representative traces.) *$P < 0.05$; **$P < 0.01$; ***$P < 0.001$; ****$P < 0.0001$; IR-DIC: infrared differential interference contrast; ML: molecular layer.

change in the neuronal excitability of granule cells in *Pomc-Cre/+::Rbfox3$^{f/f}$* mice, the intrinsic excitability of NPY-expressing GABAergic neurons was lower in *NPY-Cre/+::Rbfox3$^{f/f}$* mice and the intrinsic excitability of PV-expressing GABAergic neurons was higher in *PV-Cre/+::Rbfox3$^{f/f}$* mice compared with their controls. These results suggest that RBFOX3 may regulate GABAergic neuron-specific molecules that regulate intrinsic excitability.

No change of amplitude in the eIPSC of hippocampal granule cells with optogenetic stimulation in GABAergic neurons with *Rbfox3* deletion indicates that the number of postsynaptic receptors is not affected by RBFOX3, which is consistent with

no change of amplitude in the mIPSC of hippocampal granule cells from *Gad2-Cre/+::Rbfox3*$^{f/f}$ mice. However, the decrease in the area of the eIPSC in hippocampal granule cells with optogenetic stimulation in GABAergic neurons with *Rbfox3* deletion and a decreased PPR in hippocampal granule cells with electrical stimulation in the medial perforant path from *Gad2-Cre/+::Rbfox3*$^{f/f}$ mice suggest that sustained inhibition of GABAergic neurons with *Rbfox3* deletion was weakened, which then contributed to increased excitability of the postsynaptic granule cells and seizures. It would be of interest in future studies to examine if the reduced total amount of GABA is due to synthesis or transport problems or whether it is related to inhibitory synaptic numbers or the overall synaptic configuration.

GABAergic neurons are a diverse population and represent one type of regulatory control element for local circuits. Dysfunctional GABAergic neurons have been implicated in human neurodevelopmental disorders, including autism, schizophrenia, and epilepsy (26). Distinct GABAergic subtypes are critical for supporting network functions due to their subtype-specific synaptic connectivity (18). Such diverse physiological functions of different subtypes of GABAergic neurons could partially explain the difference in the degree of seizure phenotypes and their relationship with the deletion of *Rbfox3*. Moreover, a previous study showed that RBFOX1 mediates cell type–specific splicing in cortical GABAergic neurons (27). The different alternative splicing profiles could cause different physiological functions of GABAergic neuron subtypes and provide a partial explanation for our observations of the different seizure phenotypes in the seven subtypes of GABAergic neurons with *Rbfox3* deletion.

One limitation of studies conducted in mouse lines with a Cre driver is the cell type specificity of Cre expression. Therefore, due to the periodic expression of *Nos1-Cre* during gametogenesis, we bred *Nos1-Cre/+::Rbfox3*$^{\Delta/+}$ with *Rbfox3*$^{f/f}$ mice in order to obtain *Nos1-Cre/+::Rbfox3*$^{f/\Delta}$ and *Rbfox3*$^{f/\Delta}$ (control) mice littermates for this study (28). *Cck-Cre* is not exclusively expressed in GABAergic neurons; it is also expressed at a low level in pyramidal neurons (29). Because we eliminated the contribution of glutamatergic neurons with *Rbfox3* deletion when we examined seizure susceptibility, the lower seizure susceptibility observed in *Cck-Cre::Rbfox3*$^{f/f}$ mice was most likely due to the contribution of CCK-expressing GABAergic neurons. There was also no difference in *Gad2* mRNA levels between *Gad2*$^{Cre/+}$ and *Gad2*$^{+/+}$ mice (Dataset S1), which eliminated the possibility that GAD2 had an impact on the development of spontaneous seizures in *Gad2-Cre/+::Rbfox3*$^{f/f}$ mice. Although expression of *Npy* mRNA in *Npy*$^{Cre/+}$ mice was lower compared with levels in corresponding *Npy*$^{+/+}$ control mice (Dataset S1), we did not observe higher levels of seizure susceptibility in *Npy*$^{Cre/+}$ mice compared with their corresponding *Npy*$^{+/+}$ controls (*SI Appendix*, Fig. S8*C*).

VAMP1 is a presynaptic protein that regulates synaptic transmission and is involved in seizures (16). A previous study showed that RBFOX3 predominantly targets synaptic components (6). Our current study further solidified this concept and identified one GABAergic synaptic protein and seizure susceptibility gene, *Vamp1*, which was bound and regulated by RBFOX3. Restoration of VAMP1 in GABAergic neurons rescued seizure susceptibility and neuronal excitability of hippocampal dentate granule cells in *Gad2-Cre/+::Rbfox3*$^{f/f}$ mice, and this provides additional information on molecular mechanisms mediating seizure phenotypes due to *Rbfox3* deletion.

These mechanisms could serve as a reference for targets of drugs designed for persons with seizures with an emphasis on *RBFOX3* deletion. It would be interesting to further pursue whether VAMP1 contributes seizure susceptibility in mice with *Rbfox3* deletion in NPY-expressing GABAergic neurons. It would also be of interest for future studies to pursue how VAMP1 regulates seizures using *Vamp1* knockdown mice but not *Vamp1* conventional knockout mice due to their preweaning mortality (30).

GABAergic synapses are immature and produce depolarization in neonatal mice. Neonatal treatment with bumetanide, an inhibitor of GABA depolarization, rescued seizure phenotypes in *Gad2-Cre/+::Rbfox3*$^{f/f}$ mice. The success of this rescue and increased frequency of mIPSC in *Gad2-Cre/+::Rbfox3*$^{f/f}$ mice indicate that GABAergic neurons with *Rbfox3* deletion exhibit greater depolarization in the early stage of development, which provides evidence that bumetanide could be a potential therapeutic intervention for people with epilepsy due to *RBFOX3* deletion. Our results also support the insights that point to alterations of synaptic function and intrinsic properties of neurons as common mechanisms underlying the hyperexcitability in diverse forms of epilepsy (31).

In summary, our findings offer evidence of the crucial role for RBFOX3 in the excitation/inhibition balance in a cell type–specific manner and suggest the importance of an alternative splicing regulator in mediating brain function. Our work also provides insights into the cellular and molecular mechanisms of epileptogenesis and may offer interventions for epilepsy. This is particularly important as current therapies for epilepsy only provide symptomatic relief, are effective in only a subset of affected individuals, and are often accompanied by persistent toxic effects. Human induced pluripotent stem cells (hiPSCs) may provide a good resource to investigate the pathogenesis of epilepsy in human live neurons and brain organoids with *RBFOX3* deletion. The success of this hiPSC model may provide a platform for testing therapeutic treatments in the future.

Methods

Mice. Mice were group housed in ventilated cages, provided with food (PicoLab Rodent Diet 20; 5053) and water ad libitum, and maintained on a 12-h light/dark cycle (lights off at 8 PM). Male *Gad2-Cre/+* (*Camk2a-iCre/+*, *Pomc-Cre/+*, *PV-Cre/+*, *SOM-Cre/+*, *VIP-Cre/+*, *Npy-Cre/+*, *CR-Cre/+*, or *Cck-Cre/+*)*::Rbfox3*$^{f/+}$ mice were mated to female *Rbfox3*$^{f/f}$ mice to obtain *Gad2-Cre/+* (*Camk2a-iCre/+*, *Pomc-Cre/+*, *PV-Cre/+*, *SOM-Cre/+*, *VIP-Cre/+*, *Npy-Cre/+*, *CR-Cre/+*, or *Cck-Cre/+*)*::Rbfox3*$^{f/f}$ mice and littermate controls (*Rbfox3*$^{f/f}$). Male *Nos1-Cre/+::Rbfox3*$^{\Delta/+}$ mice were mated to female *Rbfox3*$^{f/f}$ mice to obtain *Nos1-Cre/+::Rbfox3*$^{\Delta/f}$, *Nos1-Cre/+::Rbfox3*$^{f/+}$, *Rbfox3*$^{\Delta/f}$, and *Rbfox3*$^{f/+}$ mice; "Δ" means that *Rbfox3* is deleted in all cell types. For labeling specific cell types, male *Gad2-Cre/+* (*Camk2a-iCre/+*, *Pomc-Cre/+*, *PV-Cre/+*, *SOM-Cre/+*, *VIP-Cre/+*, or *Npy-Cre/+*)*::Rbfox3*$^{f/+}$*::Ai14* mice were mated to female *Rbfox3*$^{f/+}$*::Ai14* mice to obtain *Gad2-Cre/+* (*Camk2a-iCre/+*, *Pomc-Cre/+*, *PV-Cre/+*, *SOM-Cre/+*, *VIP-Cre/+*, or *Npy-Cre/+*)*::Rbfox3*$^{f/f}$*::Ai14* mice and littermate control (*Gad2-Cre/+* [*Camk2a-iCre/+*, *Pomc-Cre/+*, *PV-Cre/+*, *SOM-Cre/+*, *VIP-Cre/+*, or *Npy-Cre/+*]*::Rbfox3*$^{+/+}$*::Ai14*) mice.

The National Taiwan University College of Medicine and the College of Public Health Institutional Animal Care and Use Committee approved all procedures. Our animal facility has earned Association for Assessment and Accreditation of Laboratory Animal Care (AAALAC) accreditation. All experiments were performed in accordance with the approved guidelines. *Rbfox3*$^{f/f}$ mice were generated by mating knockout-first and conditional-ready *Rbfox3* Homo mice (6–8) with FLPeR mice (Jackson Laboratories; stock no. 009086). *Pomc-Cre* mice (stock no. 010714), *Npy-Cre* mice (stock no. 027851), CR-Cre mice (stock no. 010774), and *Nos1-Cre* mice (stock no. 017526) were purchased from Jackson Laboratories. *PV-Cre* mice (Jackson Laboratories; stock no. 008069), *SOM-Cre* mice (Jackson Laboratories; stock no. 013044), *VIP-Cre* mice (Jackson Laboratories; stock no. 010908), and *Cck-Cre* mice (Jackson Laboratories; stock no. 012706) were provided by the laboratory of C. C. Lien (Institute of Neuroscience, National Yang Ming Chiao Tung University, Taipei, 11221, Taiwan). Detailed information of *Camk2a-iCre* (32), *Gad2-Cre* (Jackson Laboratories; stock no. 010802), and *Ai14*

Cre reporter (Jackson Laboratories; stock no. 007914) mice was mentioned in the previous study (33).

Genotyping. PCR was performed using a C1000 Touch Thermal Cycler (Bio-Rad) with SuperRed PCR Master Mix (TE-SR01; Biotools Co., Ltd.). Detailed information regarding primer sequences, PCR product sizes, and PCR cycling conditions has been described previously (6, 7, 33) and is summarized in Dataset S4.

Immunofluorescence Staining. Coronal sections (40 μm) from the hippocampus of P49 mice were used for immunofluorescence staining as previously described (7). Detailed information regarding primary and secondary antibodies is summarized in Dataset S5. In short, coronal sections were incubated with primary antibody at 4 °C overnight and then, incubated with a corresponding secondary antibody and 4′,6-diamidino-2-phenylindole (DAPI) (1:20,000; Invitrogen; D-1306) for 2 h at room temperature. Images were acquired using a Zeiss LSM780 or 880 confocal microscope (Carl Zeiss).

Spontaneous Seizure Assay. This assay was detailed in previous work (7). In brief, mice were individually and continuously video monitored in their home cages for 14 d (from P22 to P36). Seizure parameters were calculated. Experimenters were blinded to the mouse genotypes.

KA-Induced Seizure Assay. This assay was detailed in previous work (7). In brief, KA (Tocris; 0222; 22.5 mg/kg of body weight) was administered to mice by an S.C. injection, and seizure intensity was scored according to the Racine scale within 100 min after injection. Experimenters were blinded to the mouse genotypes.

Whole-Cell Recordings. Details of the methods for hippocampal slice preparation and patch clamping have been previously described (7, 34). Artificial cerebrospinal fluid (ACSF) consists of 124 mM NaCl, 3 mM KCl, 2 mM $CaCl_2$, 1 mM $MgCl_2$, 1.25 mM NaH_2PO_4, 26 mM $NaHCO_3$, and 20 mM glucose (pH 7.4, 295 mOsmol). For current-clamp recording, ACSF was supplemented with 5 mM kynurenic acid (K3375; Sigma), 5 μM SR95531 (1262; Tocris), and 1 μM strychnine (ab120416; Abcam). The internal solution contained 100 mM K-gluconate, 20 mM KCl, 0.2 mM ethylene glycol-bis(beta-aminoethyl ether)-N,N,N′,N′-tetraacetic acid (EGTA), 10 mM 4-(2-hydroxyethyl)-1-piperazineethanesulfonic acid (Hepes), 4 mM adenosine triphosphate (ATP)-Mg, 0.3 mM guanosine-5′-triphosphate (GTP)-Na, and 0.05% Neurobiotin (SP-1120; Vector Laboratories, Inc.; pH 7.2, 295 mOsmol). For voltage-clamp recording, the internal solution consisted of 100 mM $CsCH_3SO_3$, 15 mM CsCl, 2.5 mM $MgCl_2$, 10 mM Hepes, 5 mM lidocaine N-ethyl chloride (QX-314·Cl) (L1663; Sigma), 5 mM 1,2-Bis(2-aminophenoxy)ethane-N,N,N′,N′-tetraacetic acid (BAPTA)-tetracesium salt (TetraCs), 4 mM ATP-Mg, 0.3 mM GTP-Na, and 0.05% Neurobiotin (pH 7.2, 295 mOsmol). To isolate mEPSCs, 1 μM tetrodotoxin (TTX) (ab120055; Abcam), 5 μM SR95531, and 1 μM strychnine were focally applied into the ACSF bath through a perfusion valve system (VC-8 valve controller; Warner Instruments). The mIPSCs were isolated with the addition of 1 μM TTX, 5 mM kynurenic acid, and 1 μM strychnine into the ACSF bath. For patching under physiological conditions, ACSF was supplemented without any synaptic transmission blockers. ePSP recordings of the granule cells of the DG were performed with borosilicate glass electrodes with a resistance of about 4 to 6 MΩ when filled with K-gluconate–based internal solution. The amplitudes of the ePSP were recorded in the physiological condition and were evoked with a concentric bipolar stainless steel electrode (CBCMX75 [ST1]; FHC, Inc.), which was positioned in the medial perforant path of the molecular layer. Paired stimuli were delivered 50, 100, 150, 200, 500, and 1,000 ms apart, and PPRs were measured by dividing the amplitude of the second ePSP by the amplitude of the first ePSP. For the ePSP recording experiment, the amplitude of the ePSP response generated an input–output relationship to a stimulation range from 0 to 0.7 V. For the eIPSC recording experiment, *Gad2-Cre/+::Rbfox3*$^{f/f}$ mice and corresponding control mice were injected with *AAV9-mDlx-ChR2-mCherry-Fishell-3* (Addgene; 83898) in the hippocampal DG around P21, and granule cells were voltage clamped at 0 mV and recorded around P24. Blue light (465 nm) was delivered through optic fibers (Thorlabs; diameter of 200 μm) to the surface of the hippocampal DG using an light emitting diode (LED) (Doric; LEDRVP_2CH_1000) for 100 ms with the light power of 216 μW/mm^2. Experimenters were blinded to the mouse genotypes.

Real-Time qRT-PCR. Total RNA was extracted with the miRNeasy Micro kit (Qiagen; 217084). For mRNA quantification, 500 ng total RNA was converted to complementary deoxyribonucleic acid (cDNA) by SuperScript III Reverse Transcriptase (Invitrogen; 18080093). For micro ribonucleic acid (miRNA) quantification, 500 ng total RNA was added to the poly(A) tail by the A-Plus Poly(A) Polymerase Tailing Kit (CELLSCRIPT; C-PAP5104H) and converted to cDNA with the poly(T) adaptor: GCGAGCACAGAATTAATACGACTCACTATAGGTTTTTTTTTTTVN. Targeted genes were amplified by the Power SYBR Green PCR Master Mix (Applied Biosystems, 4367659). Real-time qPCR was performed with the StepOnePlus Real Time PCR System (Applied Biosystems) or the QuantStudio 5 Real-Time PCR System (Applied Biosystems). Cycle threshold (Ct) values were generated using StepOne Software version 2.3 or QuantStudio Design & Analysis Software. The expression level of each gene was normalized to *B2m* for mRNA quantification or *n-R5s195* for miRNA quantification. All primer sequences are provided in Dataset S2.

Western Blotting. Total hippocampal protein lysates were extracted from the hippocampus of P28 male *Rbfox3*$^{-/-}$ (Homo) mice and their WT counterparts and were used for further western blotting as previously described (7). Detailed information regarding primary and secondary antibodies was summarized in Dataset S5.

Mouse Surgery. Mouse pups at P0 were placed in a nitrile glove sleeve and cryoanesthetized on ice for 5 min. After hypothermia-induced anesthesia, mouse pups were transferred to a chilled homemade head-fixed stage (35). A 10-μL syringe (Hamilton) with a 32-gauge, 0.4-inch-long syringe needle was used and loaded with *AAV9-Ef1a-DIO-Rbfox3* (or *Vamp1*)*-EYFP* (1×10^{13} vector genome (vg)/mL) or *AAV9-Ef1a-DIO-EYFP* (1×10^{13} vg/mL) and 0.05% trypan blue dye solution (as a visual aid). Mouse pups were stereotactically injected (anterior–posterior [AP], +1.5 mm anterior to the lambda; medial–lateral [ML], ±0.8 mm lateral from the midline; dorsal–ventral [DV], −1.5 mm from the skull) with purified AAV into the lateral ventricles bilaterally (4 μL per hemisphere) (36). After viral injection, pups were warmed on a heating pad until their body temperatures returned to normal. Once the pups began moving, they were returned to their mother. For the eIPSC recording experiment, age P21 mice were stereotactically injected bilaterally (AP, ∼−1.40 to 1.50 mm posterior to the bregma; ML, ∼±1.15 to 1.25 mm lateral from the midline; DV, ∼−1.60 to 1.80 mm from the skull) with *AAV9-mDlx-ChR2-mCherry-Fishell-3* (Addgene; 83898; 1×10^{14} vg/mL) in the hippocampal DG (180 nL per hemisphere) using a glass micropipette.

Drug Treatment. Bumetanide (0.2 mg/kg, B3023; Sigma-Aldrich) or vehicle (0.02% dimethyl sulfoxide (DMSO) in normal saline) was administered to mice S.C. twice per day (at least 10 h of interval) from P0 to P14. Body weight of neonatal mice was measured before treatment with vehicle or bumetanide.

Stereological Cell Counting. Serial sections (40 μm) throughout the hippocampus (start from bregma −1.34 to −3.80) were collected into a 24-well culture plate. Cell numbers for each GABAergic neuron subtype were examined in every eighth section throughout the entire DG of the left hemisphere. After staining, images were acquired using a Zeiss Axio Imager M2 microscope with a 10×/0.3-NA objective (Carl Zeiss). *Z*-stack images with a 3-μm distance between consecutive images were acquired for cell counting. All stereological analyses were quantified using NIH ImageJ software with Cell Counter Plug-ins (https://imagej.net/plugins/cell-counter) and were performed by a single investigator (D.-F.H) who was blind coded via Blind Analysis Tools Plug-ins (https://imagej.net/plugins/blind-analysis-tools). An estimation of the total number of GABAergic neurons expressing the seven different subtypes (*N*) from the hippocampal DG can be made using the following formula:

$$N = \Sigma Q^{-} \times \frac{1}{ssf} \times 2,$$

where ΣQ^{-} is the total number of cells from all of the selected hippocampal DG sections and the section sampling fraction (*ssf*) is defined as the ratio between the number of sections sampled and the total number of whole serial sections of the hippocampal DG (37). Mouse genotypes were blind to the experimenters.

Statistical Analysis. All data are presented as means ± SEM with sample sizes (*n*) as shown in figures or stated in the text. Statistical analyses were performed using SigmaPlot 11 (Systat Software). Normality tests (Shapiro–Wilk) and equal variance tests were run and passed ($P > 0.05$) before parametric statistical analyses were performed. Nonparametric statistical analyses were performed if normality and equal variance tests were not passed ($P < 0.05$).

Data Availability. All study data are included in the article and/or supporting information.

ACKNOWLEDGMENTS. We thank Boting Wang, Yi-Sian Lin, I-Hsiang Li, Chen-Yu Lee, and Ivan Pochou Lai for their help with the experiments. We also thank the staff of the imaging core and the biomedical resource core at the First Core Labs, National Taiwan University College of Medicine for technical assistance. This work was funded by National Taiwan University College of Medicine and National Taiwan University Hospital Excellent Translational Medicine Research Projects 106C101-21/22 (to H.-P.H., S.S.-F.G., and H.-S.H.), 109C101-73 (to H.-P.H., S.S.-F.G., and H.-S.H.), NSC-145-51 (to H.-P.H., S.S.-F.G., and H.-S.H.), and 111C101-43 (to H.-P.H., S.S.-F.G., and H.-S.H.); National Taiwan University Hospital Grants NTUH-UN107-009 (to S.S.-F.G. and H.-S.H.) and NTUH-UN108-035 (to S.S.-F.G. and H.-S.H.); and Ministry of Science and Technology, Taiwan Grants MOST 104-2314-B-002-078-MY3 (to H.-S.H.), MOST 107-2628-B-002-004-MY3 (to H.-S.H.), and MOST 110-2314-B-002-158 (to H.-S.H.), and MOST 111-2314-B-002-256-MY2 (to H.-S.H.). We acknowledge AAV Core Facility of Academia Sinica Grant AS-CFII109-103 for the generation of recombinant AAV.

Author affiliations: [a]Graduate Institute of Brain and Mind Sciences, College of Medicine, National Taiwan University, Taipei 10051, Taiwan; [b]Graduate Institute of Medical Genomics and Proteomics, College of Medicine, National Taiwan University, Taipei 10051, Taiwan; [c]Institute of Neuroscience, National Yang Ming Chiao Tung University, Taipei 11221, Taiwan; [d]Institute of Biomedical Sciences, Academia Sinica, Taipei 11529, Taiwan; and [e]Department of Psychiatry, National Taiwan University Hospital and College of Medicine, National Taiwan University, Taipei 10051, Taiwan

1. B. K. MacDonald, O. C. Cockerell, J. W. Sander, S. D. Shorvon, The incidence and lifetime prevalence of neurological disorders in a prospective community-based study in the UK. *Brain* **123**, 665–676 (2000).
2. M. J. England, C. T. Liverman, A. M. Schultz, L. M. Strawbridge, Epilepsy across the spectrum: Promoting health and understanding. A summary of the Institute of Medicine report. *Epilepsy Behav.* **25**, 266–276 (2012).
3. E. Beghi, The epidemiology of epilepsy. *Neuroepidemiology* **54**, 185–191 (2020).
4. K. Staley, Molecular mechanisms of epilepsy. *Nat. Neurosci.* **18**, 367–372 (2015).
5. W. Duan *et al.*, Novel insights into NeuN: From neuronal marker to splicing regulator. *Mol. Neurobiol.* **53**, 1637–1647 (2015).
6. Y. S. Lin *et al.*, Neuronal splicing regulator RBFOX3 (NeuN) regulates adult hippocampal neurogenesis and synaptogenesis. *PLoS One* **11**, e0164164 (2016).
7. H. Y. Wang *et al.*, RBFOX3/NeuN is required for hippocampal circuit balance and function. *Sci. Rep.* **5**, 17383 (2015).
8. Y. S. Lin, K. T. Kuo, S. K. Chen, H. S. Huang, RBFOX3/NeuN is dispensable for visual function. *PLoS One* **13**, e0192355 (2018).
9. D. Lal *et al.*, RBFOX1 and RBFOX3 mutations in rolandic epilepsy. *PLoS One* **8**, e73323 (2013).
10. G. L. Holmes, J. L. Thompson, Effects of kainic acid on seizure susceptibility in the developing brain. *Brain Res.* **467**, 51–59 (1988).
11. R. Brenner *et al.*, BK channel beta4 subunit reduces dentate gyrus excitability and protects against temporal lobe seizures. *Nat. Neurosci.* **8**, 1752–1759 (2005).
12. J. Pallud *et al.*, Dentate gyrus and hilus transection blocks seizure propagation and granule cell dispersion in a mouse model for mesial temporal lobe epilepsy. *Hippocampus* **21**, 334–343 (2011).
13. M. Lévesque, M. Avoli, The kainic acid model of temporal lobe epilepsy. *Neurosci. Biobehav. Rev.* **37**, 2887–2899 (2013).
14. S. L. Marguet *et al.*, Treatment during a vulnerable developmental period rescues a genetic epilepsy. *Nat. Med.* **21**, 1436–1444 (2015).
15. S. M. Weyn-Vanhentenryck *et al.*, HITS-CLIP and integrative modeling define the Rbfox splicing-regulatory network linked to brain development and autism. *Cell Rep.* **6**, 1139–1152 (2014).
16. C. K. Vuong *et al.*, Rbfox1 regulates synaptic transmission through the inhibitory neuron-specific vSNARE Vamp1. *Neuron* **98**, 127–141.e7 (2018).
17. L. Tricoire, T. Vitalis, Neuronal nitric oxide synthase expressing neurons: A journey from birth to neuronal circuits. *Front. Neural Circuits* **6**, 82 (2012).
18. K. A. Pelkey *et al.*, Hippocampal GABAergic inhibitory interneurons. *Physiol. Rev.* **97**, 1619–1747 (2017).
19. A. Karagiannis *et al.*, Classification of NPY-expressing neocortical interneurons. *J. Neurosci.* **29**, 3642–3659 (2009).
20. A. Guet-McCreight, F. K. Skinner, L. Topolnik, Common principles in functional organization of vip/calretinin cell-driven disinhibitory circuits across cortical areas. *Front. Neural Circuits* **14**, 32 (2020).
21. S. B. Bausch, Axonal sprouting of GABAergic interneurons in temporal lobe epilepsy. *Epilepsy Behav.* **7**, 390–400 (2005).
22. J. Müller *et al.*, Astrocytic GABA accumulation in experimental temporal lobe epilepsy. *Front. Neurol.* **11**, 614923 (2020).
23. M. Rubinstein *et al.*, Dissecting the phenotypes of Dravet syndrome by gene deletion. *Brain* **138**, 2219–2233 (2015).
24. Q. Li, A. F. Bartley, L. E. Dobrunz, Endogenously released neuropeptide Y suppresses hippocampal short-term facilitation and is impaired by stress-induced anxiety. *J. Neurosci.* **37**, 23–37 (2017).
25. A. D. Milstein *et al.*, Inhibitory gating of input comparison in the CA1 microcircuit. *Neuron* **87**, 1274–1289 (2015).
26. K. Ramamoorthi, Y. Lin, The contribution of GABAergic dysfunction to neurodevelopmental disorders. *Trends Mol. Med.* **17**, 452–462 (2011).
27. B. Wamsley *et al.*, Rbfox1 mediates cell-type-specific splicing in cortical interneurons. *Neuron* **100**, 846–859.e7 (2018).
28. R. L. Leshan, M. Greenwald-Yarnell, C. M. Patterson, I. E. Gonzalez, M. G. Myers Jr., Leptin action through hypothalamic nitric oxide synthase-1-expressing neurons controls energy balance. *Nat. Med.* **18**, 820–823 (2012).
29. H. Taniguchi *et al.*, A resource of Cre driver lines for genetic targeting of GABAergic neurons in cerebral cortex. *Neuron* **71**, 995–1013 (2011).
30. A. M. Nystuen, J. K. Schwendinger, A. J. Sachs, A. W. Yang, N. B. Haider, A null mutation in VAMP1/synaptobrevin is associated with neurological defects and prewean mortality in the lethal-wasting mouse mutant. *Neurogenetics* **8**, 1–10 (2007).
31. J. O. McNamara, Emerging insights into the genesis of epilepsy. *Nature* **399**(6738 suppl.), A15–A22 (1999).
32. E. Casanova *et al.*, A CamKIIalpha iCre BAC allows brain-specific gene inactivation. *Genesis* **31**, 37–42 (2001).
33. C. Y. Lin *et al.*, Analysis of genome-wide monoallelic expression patterns in three major cell types of mouse visual cortex using laser capture microdissection. *PLoS One* **11**, e0163663 (2016).
34. M. Y. Chou *et al.*, Mouse hybrid genome mediates diverse brain phenotypes with the specificity of reciprocal crosses. *FASEB J.* **36**, e22232 (2022).
35. S. Y. Chen, H. Y. Kuo, F. C. Liu, Stereotaxic surgery for genetic manipulation in striatal cells of neonatal mouse brains. *J. Vis. Exp.* **137**, 57270 (2018).
36. J. Y. Kim, S. D. Grunke, Y. Levites, T. E. Golde, J. L. Jankowsky, Intracerebroventricular viral injection of the neonatal mouse brain for persistent and widespread neuronal transduction. *J. Vis. Exp.* **51863**, 51863 (2014).
37. K. A. Dorph-Petersen, D. A. Lewis, Stereological approaches to identifying neuropathology in psychosis. *Biol. Psychiatry* **69**, 113–126 (2011).